Title
Chromatic matching in a plasma undulator

Permalink
https://escholarship.org/uc/item/1zk8g212

Journal
Physics of Plasmas, 26(11)

ISSN
1070-664X

Authors
Djordjević, BZ
Benedetti, C
Schroeder, CB
et al.

Publication Date
2019-11-01

DOI
10.1063/1.5120868

Peer reviewed

Chromatic matching in a plasma undulator

B.Z. Djordjević,[1,2] C. Benedetti,[2] C.B. Schroeder,[2,3] and E. Esarey[2]

[1] *Department of Physics, University of California, Berkeley, CA, 94720, USA*

[2] *BELLA Center, Lawrence Berkeley National Laboratory, Berkeley, CA, 94720, USA*

[3] *Department of Nuclear Engineering, University of California, Berkeley, CA, 94720, USA*

The principle of chromatic matching, i.e., using two laser modes of different geometric modes numbers and of different colors such that they copropagate at the same group velocity, is proposed in order to realize the plasma undulator concept. Chromatic matching allows one to overcome group velocity slippage, whereby lower-order modes outrun higher-order ones, allowing for extended interaction lengths. The dephasing limit can be mitigated by using a special tapering of the plasma channel such that the electron bunch propagates in phase with the laser mode as well as maintain constant undulator frequency. In addition, controlled dephasing is proposed as a means to induce chirp in the generated x-ray spectrum.

I. INTRODUCTION

High energy radiation sources are an important technological tool for studying fundamental physical processes.[1] Modern light sources such as those at LCLS[2] and DESY[3] are able to resolve matter up to the molecular level at near real-time with high repetition rates.[4] Key enabling technologies are synchrotrons and more specifically the Free Electron Laser (FEL),[5] which amplifies synchrotron radiation from an oscillating, relativistic charged electron bunch. The wavelength of the synchrotron radiation emitted by a particle or bunch oscillating in an undulator is $\lambda_s = \lambda_u(1 + K^2/2)/(2\gamma_0^2)$, where γ_0 is the relativistic Lorentz factor of the electron, $\lambda_u = 2\pi/k_u = 2\pi c/\omega_u$ is the undulator wavelength, and K is the strength parameter of the undulator. In traditional systems, these oscillations are driven by conventional magnets with undulator length scales on the order of a millimeter at the smallest, requiring very energetic electron bunches to generate hard X-rays, i.e., $\gamma_0 \sim 10,000$.[6] Synchrotron radiation can be produced by both circular as well as linear accelerators, but in both cases the scales and costs involved are problematic and cannot keep up with user demand. One possible way to reduce the size of synchrotron structures is to use a plasma-based system.

The earliest plasma-based light sources utilized radiation from betatron oscillations.[7] This approach has been tested in experiment and applied to high-density plasma observations as a backlight prober.[8] Another plasma-based approach is to use a laser to induce the desired oscillations in the trailing electron bunch.[9,10] This approach involves injecting a laser pulse off-axis into a parabolic plasma channel so that the wake creates an undulator-like structure for the trailing electron bunch. Yet another approach is to use the superposition of two laser pulses of different mode numbers and to use the beating between the modes to create the undulator structure.[11] Higher-order mode content at several Watts of power can be readily generated using off-axis pumping.[12–14] This provides greater flexibility in controlling the frequency of the output radiation as the undulator frequency is a function of the difference between the mode numbers. One noticeable limitation of this concept is that laser pulses of different mode numbers propagate at different group velocities, extinguishing the effect after several tens of oscillations.[15] One solution to this problem is chromatic matching, i.e., color tuning, where two modes of slightly different frequencies propagate at the same group velocity.[16] These plasma-based approaches are typically envisioned as being coupled to a Laser-Plasma Accelerator (LPA), yielding a radiation source with an extremely compact footprint.

In an LPA, a short but intense laser pulse ($I \gtrsim 10^{18}$ W/cm^2) propagates through a plasma and generates a plasma wave.[17–19] To maximize the wake amplitude, the length of the laser pulse, L, is chosen to be approximately equal to the plasma wavelength, $\lambda_p = 2\pi/k_p = 2\pi c/\omega_p$, where c is the speed of light, $\omega_p^2 = 4\pi n_0 q_e^2/m_e$ is the plasma frequency, n_0 is the on-axis plasma density, and q_e and m_e are the fundamental electron charge and mass. The wake is created and driven by the ponderomotive force, $F \simeq -m_e c^2 \nabla a^2$, where $a = q_e A/(m_e c^2)$ is the normalized laser vector potential, and A is the vector potential of the laser field. Diffraction of a laser pulse in vacuum is described by the Rayleigh length, $Z_R = \pi r_0^2/\lambda$, where r_0 is the initial laser spot-size at $1/e^2$ the intensity and $\lambda = 2\pi/k = 2\pi c/\omega$ is the laser wavelength.

There are several important limitations to the LPA concept which can be defined by relevant length scales. In the weakly relativistic limit, $a^2 \ll 1$, they are the diffraction limit, which scales according to $L_{\rm diff} \sim Z_R$, dephasing, $L_{\rm deph} \sim \lambda_p^3/\lambda^2$, and energy depletion, $L_{\rm depl} \sim \lambda_p^3/(\lambda a)^2$, i.e., redshifting in the drive laser. In addition, if multiple laser modes are employed, another limitation is mode slippage, $L_{\rm slip} \sim L(kr_0)^2/(2|m_1 - m_2|)$, where modes, Hermite-Gaussian in this case, of different geometric mode numbers, e.g., m_1 and m_2, slip apart. The standard approach to addressing diffraction is to use a parabolic plasma channel where the transverse density profile is matched to the laser spot-size r_s. For dephasing, where the electron bunch outruns the laser, $\beta_{\rm bunch} \approx 1 > \beta_{\rm laser} \simeq 1 - k_p^2/(2k^2)[1 + 4(m_{1,2} + 1)/(k_p r_0)^2]$, where $\beta = v/c$, one uses a longitudinal density taper that compresses the plasma wavelength in phase with the electron.

Energy depletion can be addressed by using a staged LPA system. Mode slippage can be addressed by chromatic matching of the different modes.[16]

In this paper we propose the use of chromatic matching in a plasma undulator, following similar analysis as carried out in Ref. 16. Higher-order modes, in either the Laguerre or Hermite-Gaussian bases, propagate at lower velocities, such that $\beta_m = 1 - k_p^2/(2k_m^2)[1 + 4(m + 1)/(k_p r_0)^2]$, where k_m is the wave number of the m-th mode. Chromatic matching is the principle of choosing different colors for different laser pulses of different geometric mode numbers such that they copropagate, i.e., $k_1 \neq k_2$ and $m_1 \neq m_2$ but $\beta_1 = \beta_2$. This eliminates mode slippage between the modes and allows for an interaction length much larger than L_{slip}, enabling for a much more intense X-ray source. Likewise, this source is tunable in that we can vary the synchrotron frequency by choosing different mode number combinations. This is valid for both low energy and high energy bunches, with the later requiring a special density tapering to guide the bunch over longer distances with constant ω_u. Lastly, we can adjust the tapering of the density profiles to induce a chirp in the emitted spectrum.

This paper is organized as follows. In Sec. II of this paper we present the general solution of the paraxial wave equation in a parabolic plasma channel as well as the effects of mode beating and color tuning. In Sec. III we present the wakefields in the Hermite-Gaussian basis for color-tuned modes. In Sec. IV we provide preliminary results for the propagation of a low-energy electron bunch with a velocity matched to the group velocity of the laser and the emitted radiation. In Sec. V we present results for a highly relativistic electron bunch in a color-tuned plasma undulator by considering a density taper in the background plasma channel. In Sec. VI we explore the possibility of using modified tapering to induce a controlled chirp in the synchrotron radiation. In Sec. VII, we present a summary of our theory and results and propose potential experimental implementations and future prospects.

II. HIGHER-ORDER LASER MODE PROPAGATION

A standard approach to describing laser propagation through a plasma is to use the paraxial approximation, such that $|k\partial_z a| \gg |\partial_z^2 a|$, where z is the propagation variable, as well as assuming a low-power and low-intensity limit of $|a|^2 \ll 1$:

$$\nabla_\perp^2 a + 2ik\partial_z a = k_p^2(n/n_0)a, \qquad (1)$$

where we have the Laplacian $\nabla_\perp^2 = \partial_x^2 + \partial_y^2$ in Cartesian coordinates. For a parabolic channel, the plasma density can be characterized by radius R:

$$n(x,y) = n_0\left[1 + (x^2 + y^2)/R^2\right], \qquad (2)$$

where x, y are the transverse coordinates.

In both Eqs. (1) and (2) we neglect the effects of relativistic self-focusing and ponderomotive self-channeling. A low-intensity Gaussian pulse injected into a parabolic channel which propagates with constant spot size $r_s = r_0$ and peak intensity a_0^2 if $R = k_p r_0^2/2$ is said to be matched.[19] This also holds true for all individual higher-order modes in the Hermite-Gaussian basis. All subsequent analysis can also be done in cylindrical coordinates, for which the basis is the Laguerre-Gaussian modes. However, only the Cartesian formulation will be used in this paper.

A. Copropagation of Hermite-Gaussian modes

In the Cartesian basis we can express the transverse envelope profile of individual laser modes as

$$a_{m,n}(x,y) = \frac{C_{m,n}}{(m!n!2^{m+n})^{\frac{1}{2}}} H_m\left(\frac{\sqrt{2}x}{r_0}\right) H_n\left(\frac{\sqrt{2}y}{r_0}\right)$$
$$\times\, e^{-\frac{(x^2+y^2)}{r_0^2}} e^{i(\phi_{mn}+\phi_0)}, \qquad (3)$$

where $C_{m,n}$ is the amplitude contribution of mode (m, n) to the radiation field, $H_m(\cdot)$ is the Hermite polynomial of order m, the phase contribution from the dispersion relation is given by $\phi_{m,n} = (-k_p^2/2k)[1 + 4(m + n + 1)/(k_p r_0)^2]z$, and the initial phase is ϕ_0. From this we derive the phase velocity of the mode:[20]

$$\frac{v_{p,mn}}{c} = 1 + \frac{k_p^2}{2k^2}\left[1 + \frac{4(m+n+1)}{(k_p r_0)^2}\right]. \qquad (4)$$

As noted previously, an individual laser mode with a matched spot size will propagate without variation in intensity down a plasma channel. However, two overlapping matched modes will interfere and induce beating. For two modes, a_1 and a_2, of arbitrary mode numbers, the intensity takes the following form:

$$|a|^2 = |a_1 + a_2|^2 = |a_1|^2 + |a_2|^2 + a_1 a_2^* + a_1^* a_2, \qquad (5)$$

where for linearly polarized, Hermite-Gaussian modes of the same color k we have:

$$k_{\mathrm{beat}} = [(m_1 + n_1) - (m_2 + n_2)]/Z_R. \qquad (6)$$

If the sum of the mode numbers for each mode is not equal, there will be a beating term with a characteristic wavelength of $\lambda_{\mathrm{beat}} = 2\pi/k_{\mathrm{beat}}$. For certain applications one can choose mode numbers such that they cancel out, i.e., $m_1 + n_1 = m_2 + n_2$, and in this case there will be no beating.[16]

B. Color tuning for copropagation

As mentioned before, laser pulses of different mode numbers propagate at different group velocities and

thereby slip apart, lower-order modes moving faster than higher-order ones. The group velocity of an individual laser mode can be derived from the following relation, $v_g/c = \partial\omega/\partial k$. For a Hermite-Gaussian mode the group velocity is:

$$\frac{v_{g,mn}}{c} = 1 - \frac{k_p^2}{2k_{m,n}^2}\left[1 + \frac{4(m+n+1)}{(k_p r_0)^2}\right], \qquad (7)$$

where $k_{m,n}$ is the wavenumber of a mode $a_{m,n}$. The characteristic slippage length between two higher-order modes is:

$$L_{s,mn} \approx L(kr_0)^2/(2|(m_1+n_1)-(m_2+n_2)|). \qquad (8)$$

By setting the group velocities of two different modes equal to one another, we can derive a simple relation for the frequencies, i.e., the colors, of two modes:

$$k_2 = k_1\sqrt{\frac{1+\kappa^2(m_2+n_2+1)}{1+\kappa^2(m_1+n_1+1)}}, \qquad (9)$$

where $\kappa = 2/(k_p r_0)$. This is equivalent to Eq. (24) in Ref. 16. As we can deduce from this equation, in order for a higher-order mode to propagate at the same group velocity as a lower-order mode, it will need to have a slightly higher frequency, assuming that $\kappa < 1$. Using two colors modifies Eq. (6), giving us instead,

$$k_{\text{beat}} = |k_2[\kappa^2(m_1+n_1)+1] - k_1[\kappa^2(m_2+n_2)+1]| \\ \times 2/(\kappa^2 k_1 k_2 r_0^2). \qquad (10)$$

However, it is important to note that color-tuning is sensitive and so one only has a margin of error of a few percent $\Delta k/k_m$ before significant slipping occurs, where we have simplified Eq. (9) to consider just one higher-order mode m

$$k_m = k_0\sqrt{[1+\kappa^2(m+1)](1+\kappa^2)}. \qquad (11)$$

This is visualized in Fig. 1, where we have plotted $e^{-[v_{g,00}-v_{g,m0}(\tilde{k})]^2 L_{s,m0}^2/(2L^2)}$, which tells us the relative copropagation, i.e., the intensity of the beating term between a Gaussian mode and a mode m over the characteristic slippage length, if the color $\tilde{k}$ of mode m is off relative to its color-tuned value k_m. The higher the mode the less sensitive it is to tuning errors with respect to slippage.

III. WAKEFIELD CALCULATIONS OF COLOR TUNED MODES

In the linear regime, the response of the wake can be determined from the normalized electrostatic potential,

$\phi = q_e\Phi/m_e c^2$, where Φ is the scalar potential, and the density perturbation to the wake, $\delta n/n_0$, are governed
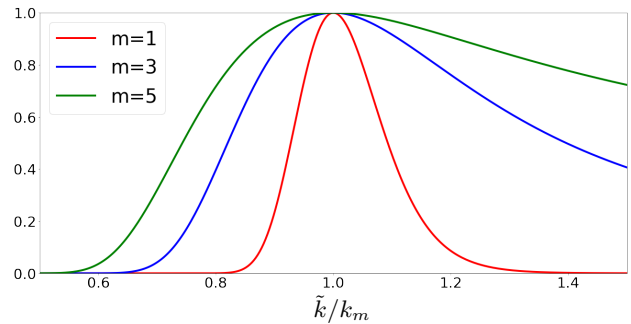

FIG. 1. Plot of the relative copropagation factor between a Gaussian mode and a mode $m=1$ (red), $m=3$ (blue), and $m=5$ (green) as a function of relative wavenumber $\tilde{k}/k_m$.

by the equations[19]

$$\left(\frac{\partial^2}{\partial\zeta^2} + k_p^2\right)\phi = k_p^2\frac{a^2}{2}, \qquad (12)$$

$$\left(\frac{\partial^2}{\partial\zeta^2} + k_p^2\right)\frac{\delta n}{n_0} = \frac{\nabla^2 a^2}{2}, \qquad (13)$$

where $\zeta = z - v_{g,00}t$ is the comoving variable, v_{g0} corresponds to the group velocity of the lowest order mode, and we assume a broad channel, i.e., $k_p R \gg 1$. From Eq. (12) we can write the Green's function solution:

$$\phi = \frac{k_p}{4}\int_{\infty}^{\zeta} d\zeta' \sin[k_p(\zeta-\zeta')]|\hat{a}(x,y,\tau,\zeta')|^2, \qquad (14)$$

where $\tau = ct$ is the propagation variable, $\hat{a}(x,y,\tau,\zeta) = a(x,y,\tau)g(\zeta)$, $g(\zeta) = \exp[-(\zeta-\zeta_0)^2/L^2]$ is the longitudinal profile of the laser pulse (assumed Gaussian) and ζ_0 is the laser centroid position. The transverse electric field is given by

$$E_\perp/E_0 = -k_p^{-1}\nabla_\perp\phi. \qquad (15)$$

For a general superposition of a Gaussian pulse with a higher-order mode of arbitrary mode number m but $n = 0$, and to each mode a specific wavelength, we have the following for the intensity profile and the odd harmonics of the electric fields, i.e., $m = 1, 3, 5, ...$,

$$|a|^2 = \left[C_0^2 e^{\frac{2(\zeta-\delta\beta\tau)^2}{L^2}} + \frac{2^{1-\frac{m}{2}}}{\sqrt{m!}} C_0 C_m H_m(\tilde{x}) e^{\frac{\zeta^2+(\zeta-\delta\beta\tau)^2}{L^2}} \cos(k_{u,m}\tau) + \frac{2^{-m}}{m!} C_m^2 H_m(\tilde{x})^2 e^{\frac{2(\zeta-\delta\beta\tau)^2}{L^2}} \right] e^{-(\tilde{x}^2+\tilde{y}^2)}, \quad (16)$$

$$\frac{E_x}{E_0} = \frac{4}{\sqrt{2}} \mathcal{C} e^{-(\tilde{x}^2+\tilde{y}^2)} \left\{ C_0^2 \tilde{x} \sin(k_p\zeta) + \frac{2^{-m}}{m!} C_m^2 H_m(\tilde{x}) \left[2m H_{m-1}(\tilde{x}) - \tilde{x} H_m(\tilde{x}) \right] \sin[k_p(\delta\beta\tau - \zeta)] \right.$$
$$\left. + \frac{2^{-m/2}}{\sqrt{m!}} C_0 C_m e^{-\frac{\delta\beta^2\tau^2}{2L^2}} \left[2m H_{m-1}(\tilde{x}) - 2\tilde{x} H_m(\tilde{x}) \right] \cos(k_{u,m}\tau) \sin[k_p(\delta\beta\tau - 2\zeta)/2] \right\}, \quad (17)$$

$$\frac{E_y}{E_0} = \mathcal{C} e^{-(\tilde{x}^2+\tilde{y}^2)} \tilde{y} \left\{ C_0^2 \sin(k_p\zeta) - \frac{2^{-m}}{m!} C_m^2 H_m^2(\tilde{x}) \sin[k_p(\delta\beta\tau - \zeta)] \right.$$
$$\left. - \frac{2^{1-\frac{m}{2}}}{\sqrt{m!}} C_0 C_m e^{-\frac{\delta\beta^2\tau^2}{2L^2}} H_m(\tilde{x}) \cos(\omega_{k_n}t) \sin[k_p(\delta\beta\tau - 2\zeta)/2] \right\}, \quad (18)$$

$$\frac{E_z}{E_0} = -\mathcal{C} e^{-(\tilde{x}^2+\tilde{y}^2)} k_p r_0 \left\{ C_0^2 \cos(k_p\zeta) + \frac{2^{-m}}{m!} C_m^2 H_m^2(\tilde{x}) \cos[k_p(\delta\beta\tau - \zeta)] \right.$$
$$\left. + \frac{2^{1-m/2}}{\sqrt{m!}} C_0 C_m H_m(\tilde{x}) e^{-\frac{\delta\beta^2\tau^2}{2L^2}} \cos(k_{u,m}\tau) \cos[k_p(\delta\beta\tau - 2\zeta)/2] \right\}, \quad (19)$$
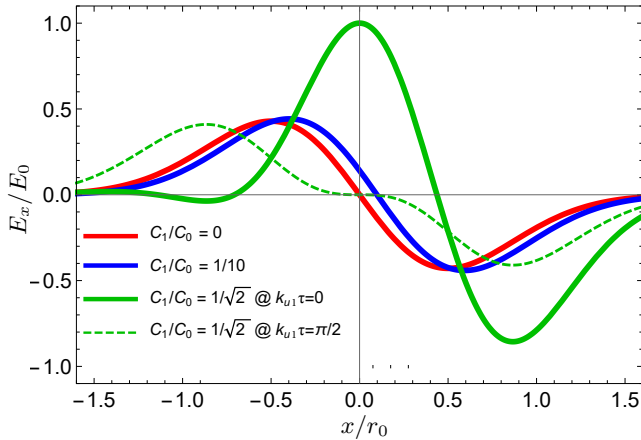

FIG. 2. Lineouts of the transverse electric field E_x/E_0 for the superposition of $m = 0$ and $m = 1$ modes with $C_0 = 0.1$ and $\zeta = -\pi/2$. Only Gaussian field $m = 0$ (red), two modes $m = 0$ and $m = 1$ with coefficient ratio $C_1/C_0 = 1/10$ (blue), $m = 0$ and $m = 1$ with coefficient ratio $C_1/C_0 = 1/\sqrt{2}$ at $k_{u,1}\tau = 0$ (solid green), and $m = 0$ and $m = 1$ with coefficient ratio $C_1/C_0 = 1/\sqrt{2}$ at $k_{u,1}\tau = \pi/2$ (dashed green).

where $\tilde{x} = \sqrt{2}x/r_0$, $\tilde{y} = \sqrt{2}y/r_0$, $\delta\beta = \beta_{g0} - \beta_{gm}$, $\mathcal{C} = \frac{1}{4} e^{-k_p^2 L^2/8} (k_p L) \sqrt{\pi/2}/(k_p r_0)$, and

$$k_{u,m} = \left| k_m(\kappa^2 + 1) - k_0[\kappa^2(m+1) + 1] \right| /(k_m Z_R), \quad (20)$$

is the undulator frequency. The Rayleigh range is defined with respect to the color, i.e., the wave number k_0, of the Gaussian mode, i.e., $Z_R = k_0 r_0^2/2$, and k_m is the wavenumber of m-th higher-order mode defined by Eq. (11). If two modes are mistuned such that $k_m \neq k_0$ there will be slippage. An example of the transverse fields can be seen in Figs. 2 and 3. In Fig. 2 we have plotted E_x/E_0 for four different circumstances of the superposition of the $m = 0$ and $m = 1$ modes with $C_0 = 0.1$ and $\zeta = -\pi/2$, when $C_1 = 0$ (red), $C_1/C_0 = 1/10$ (blue), $C_1/C_0 = 1/\sqrt{2}$ at $k_{u,1}\tau = 0$ (solid green), and $C_1/C_0 = 1/\sqrt{2}$ at $k_{u,1}\tau = \pi/2$ (dashed green). $C_1/C_0 = 1/10$ corresponds to a modest perturbation of the transverse field while $C_1/C_0 = 1/\sqrt{2}$ corresponds to when the electric field gradient is zero on-axis, i.e., $k_{\beta x} = 0$, where $k_{\beta x}$ is the betatron wave number in the x-direction. In Fig. 3 are plotted the intensity (color) and direction (vectors) of the $m = 1$ case when $C_1/C_2 = 1/\sqrt{2}$ at six instances in the modes' evolution: (a) $k_{u,1}\tau = 0$, (b) $k_{u,1}\tau = \pi/4$, (c) $k_{u,1}\tau = 3\pi/8$, (d) $k_{u,1}\tau = \pi/2$, (e) $k_{u,1}\tau = 5\pi/8$, and (f) $k_{u,1}\tau = 3\pi/4$.

The field equations can be linearized for particles near the axis of propagation of the laser. For example, for the superposition of a first-order mode ($m = 1$) and a Gaussian pulse ($m = 0$), the wakefields is,

$$\frac{E_x}{E_0} \approx \frac{4}{\sqrt{2}} \mathcal{C} \left\{ \tilde{x} \left[C_0^2 \sin(k_p\zeta) - g(m)^2 C_1^2 \sin[k_p(\delta\beta\tau - \zeta)] \right] + \sqrt{2} C_0 C_1 e^{-\frac{\delta\beta^2\tau^2}{2L^2}} \cos(k_{u,m}\tau) \sin[k_p(\delta\beta\tau - 2\zeta)/2] \right\}, \quad (21)$$
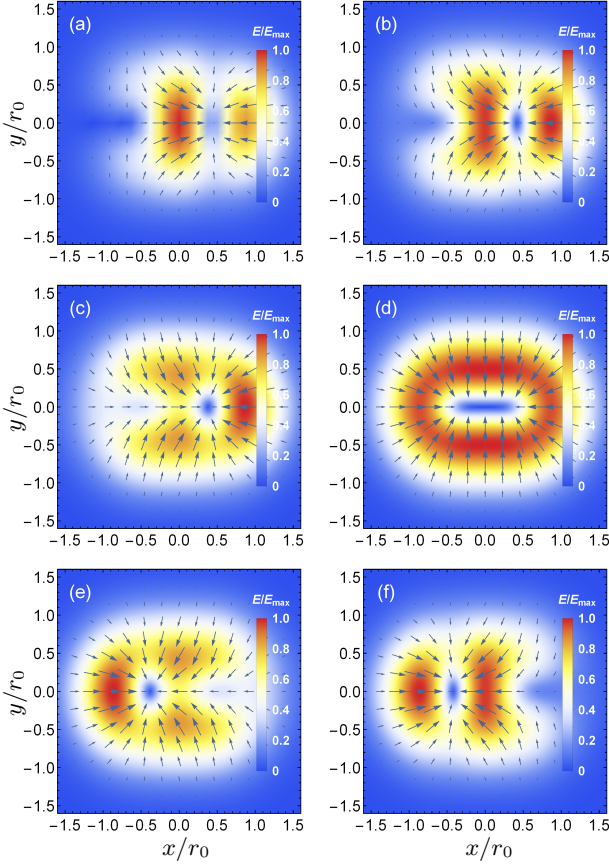
FIG. 3. The transverse electric fields $E_\perp/E_0$, where the color corresponds to the intensity of the field and the vectors to the direction, at several instances of their time evolution: (a) $k_{u,1}\tau = 0$, (b) $k_{u,1}\tau = \pi/4$, (c) $k_{u,1}\tau = 3\pi/8$, (d) $k_{u,1}\tau = \pi/2$, (e) $k_{u,1}\tau = 5\pi/8$, and (f) $k_{u,1}\tau = 3\pi/4$.

$$\frac{E_y}{E_0} \approx \frac{4}{\sqrt{2}}\mathcal{C}C_0^2\tilde{y}\sin(k_p\zeta), \qquad (22)$$

$$\frac{E_z}{E_0} \approx -4\mathcal{C}C_0^2(k_pr_0)\cos(k_p\zeta), \qquad (23)$$

where $g(m) = \sqrt{\frac{\pi}{m!}}\frac{2^{m/2}m}{\Gamma(m/2)}\frac{\pi}{\sin(\pi m/2)}$, e.g., $g(1) = \sqrt{2}$, where Euler's reflection formula $\Gamma(z)\Gamma(1-z) = \pi/\sin(\pi z)$ has been used. Analogous expressions can be generated for the $m = 2, 4, 6, ...$ modes but such modes will not contribute to the longitudinal, accelerating field and so are of less interest.

From the linear equations we can derive approximate values for the betatron frequencies of the trailing bunch as well as the characteristic undulator betatron and strength parameters, a_β and a_u. The betatron wave numbers for mode number m are

$$k_{\beta x}^2 \approx 2\sqrt{2}\mathcal{C}[C_0^2 - g(m)^2C_1^2\sin(k_p(\zeta - \delta\beta\tau)]k_p^2/\gamma_0, \qquad (24)$$

$$k_{\beta y}^2 \approx 2\sqrt{2}\mathcal{C}C_0^2k_p^2/\gamma_0, \qquad (25)$$

and the betatron wave number gives the betatron strength parameters $a_{\beta x} = \gamma_0k_{\beta x}x_b$ and $a_{\beta y} = \gamma_0k_{\beta y}y_b$ for an electron or bunch of energy γ_0, where x_b and y_b are the betatron oscillation amplitudes. The undulator strength parameter for arbitrary mode m can be written as,

$$a_u(k_m) \approx \sqrt{\frac{8}{\pi}}\frac{k_pk_{u,m}}{k_{\beta x}^2 - k_{u,m}^2}\mathcal{C}C_0C_1g(m)e^{-\delta\beta^2\tau^2/(2L^2)}$$
$$\times k_pr_0\cos(k_{u,m}\tau)\sin\left[\frac{1}{2}k_p(\delta\beta\tau - 2\zeta)\right], \qquad (26)$$

where a_u is a function of k_m. The undulator and betatron strength parameters modify the emission frequency:

$$\omega_s = 2\gamma_0\omega_{u,m}/(1 + a_u^2/2 + a_\beta^2/2), \qquad (27)$$

where $\omega_{u,m} = k_{u,m}c$. For simplicity, we will neglect motion in the y-plane in the following analysis, i.e., $a_\beta = a_{\beta x}$.

As we can see in Eqs. (24) and (25), we can control not only the strength of the undulation but also the betatron oscillations. For example, setting $C_0 = \sqrt{2}C_1$ would minimize betatron oscillations in the x-plane for the $m = 1$ mode. A similar approach can be taken in the y-plane by including a second $n = 1$ Hermite-Gaussian mode (or by using cylindrical, Laguerre-Gaussian modes). The ability to control k_β independently of k_u would best be utilized as a means to match the undulator channel to the injected beam. However, we can see in both Eqs. (24) and (26) a time dependence that decays on a length scale $\sqrt{2}L/\delta\beta$, which corresponds to the slippage length $L_{s,mn}$. Once the modes slip apart the bunch will oscillate between frequencies of $\sqrt{2\sqrt{2}\mathcal{C}(C_0^2 - 2C_1^2)/\gamma_0}\omega_p$ and $\sqrt{2\sqrt{2}\mathcal{C}(C_0^2 + 2C_1^2)/\gamma_0}\omega_p$ and undulator radiation at the resonant frequency will be suppressed.

IV. LOW-ENERGY, COLOR-TUNED SYNCHROTRON SOURCE

As a proof-of-concept, we examine a low-energy case for a single electron in which $\gamma_0 = 1/\sqrt{1 - \beta_{g,00}^2}$, i.e., the energy of the electron bunch corresponding to the velocity of the lowest-order, fastest, mode in consideration. In this example we are not limited by dephasing between the guided electron and the laser mode. Using the fields described in Eqs. (17) - (19), we can determine the trajectory of a test electron and the emitted radiation.

Plotted in Fig. 4 are three cases of electron motion, one for which the modes are the same color and thereby propagate at different velocities with the electron initialized at $x_0 = 0$ (dashed red), a similar case but initialized at $x_0 = a_u(k_0)/(\gamma_0k_{u,0})$ (solid red), and a final case in which the modes are color-tuned and initialized at $x_1 = a_u(k_1)/(\gamma_0k_{u,1})$ (solid blue). In this example the

on-axis density is $n_0 = 10^{18}$ cm^{-3}, laser mode amplitudes are $C_0 = 0.003$ and $C_1 = C_0/\sqrt{2}$, laser spot-size is $k_p r_0 = 5$, centroid position $k_p \zeta_0 = -\pi/2$, and $\gamma_0 = 37.83$. In Fig. 4 we can see how the non-tuned, $x_0 = 0$, electron initially oscillates at the undulator frequency but eventually this behavior decays into simple betatron motion as the wakes of the two modes slip apart. For the color-tuned case the modes never separate and we have simple oscillatory motion. At $\tau = 81 Z_R$ we have demarcated the slippage length scale $L_{s,1}$. The trajectories have different amplitudes but the laser energy is the same in all three cases. We initialized the non-tuned modes at $x(0) = x_0$, since for them to have the same amplitude as the color-tuned case would require four times as much power.

Of primary interest is the radiation spectrum emitted by such trajectories. Considering the oscillations first only up to the slippage length, we calculate the radiation emitted by solving the far-field approximation of the Liénard-Wiechart potentials:

$$\frac{d^2 I}{d\omega d\Omega} = \frac{q_e^2 \omega^2}{4\pi^2 c} \left| \sum_{n=1}^{N} \int_{-\infty}^{\infty} [\mathbf{s} \times (\mathbf{s} \times \boldsymbol{\beta}_n)] \, e^{-i\omega(t - \mathbf{s}\cdot\mathbf{x}_n/c)} dt \right|^2,$$
(28)

where $d^2 I / d\omega d\Omega$ is the energy radiated per frequency ω per solid angle Ω, N is the number of electrons in consideration, $\mathbf{s} = [0, \sin(\theta), \cos(\theta)]$, θ is the polar angle with respect to the axis (we will only be considering radiation emitted in a single plane), $\boldsymbol{\beta}_n = (\beta_x, \beta_y, \beta_z)$ are the velocity components of particle n and relate to the momentum via $p = \gamma_0 m_e c \beta$, and $\mathbf{x}_n = (x, y, z)$ is the position of particle n. We solve for the radiation field numerically by discretizing the time integral accordingly.

The emitted radiation of a single electron can be further characterized, assuming constant strength parameter a_u, linear polarization, and considering only the fundamental emission line near axis. $r \approx 0$. The natural bandwidth is $\Delta\omega/\omega = 1/N_u$, where $N_u = \tau_{\text{end}}/\lambda_\beta$ is the number of betatron periods over the total propagation distance. The total number of photons emitted by a single electron propagating through an undulator is[10]

$$N_p = \pi \alpha_f \frac{a_u^2}{1 + a_u^2/2} |J_0(\chi) - J_1(\chi)|^2,$$
(29)

where $\alpha = q_e^2/(\hbar c)$ is the fine structure constant, J_0 and J_1 are the zeroth and first-order Bessel functions, and $\chi = a_u^2/[4(1 + a_u^2/2)]$. The collimation angle for achieving natural bandwidth of emitted radiation is given by

$$\theta_n = \frac{1}{\gamma_0} \sqrt{\frac{1 + a_u^2/2}{N_u}}.$$
(30)

In addition to the trajectories depicted in Fig. 4 for mode $m = 1$ we also consider the trajectories for $m = 3$. The wavelengths in consideration are $\lambda_0 = 815$ nm for the Gaussian and non-tuned modes, $\lambda_1 = 764$ nm and $\lambda_3 = 685$ nm for the color-tuned modes. The spectra, normalized to $I_0 = q_e^2/(4\pi^2 c)$, are integrated up to
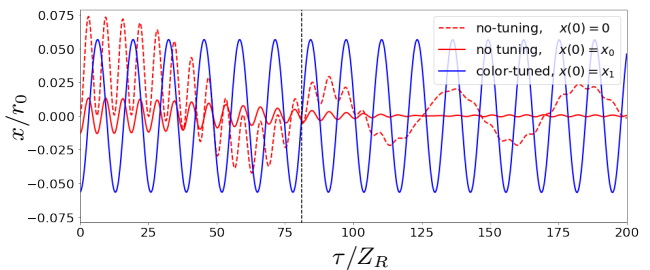

FIG. 4. Plot of the trajectories of an electron propagating in the wake of an $m = 0$ and $m = 1$ laser driver. Trajectory in the wake of non-tuned modes (dashed red) initialized at $x_0 = 0$, in the wake of non-tuned modes (solid red) initialized at $x_0 = a_u(k_0)/(\gamma_0 k_{u,0})$, and in the wake of color-tuned modes (blue) that are properly initialized at $x_1 = a_u(k_1)/(\gamma_0 k_{u,1})$.

$L_{s,1} \approx 81 Z_R$ for the $m = 1$ trajectories and $L_{s,3} \approx 27 Z_R$ for $m = 3$, all initialized at $x_0 = a_u(k_m)/(\gamma_0 k_{u,m})$, are plotted in Fig. 5a versus $\omega/2\gamma_0^2\omega_1$. For the same propagation distance radiation, the spectrum is more intense though at a lower frequency for a color-tuned pulse (blue) as opposed to one that is not (red). However, the lower frequency for an $m = 1$ color-tuned pulse can be overcome by increasing the mode number, e.g., $m = 3$. If integrated to the same propagation distance, a color-tuned $m = 3$ pulse (green) has the same intensity as an $m = 1$ pulse (blue) while gaining in frequency, while the decreasing slippage length of non-tuned modes leads to decreasing intensities (purple). The primary benefit of the color-tuned schema is that there is no restriction with respect to slippage. This is visualized in Fig. 5b, where we have integrated the spectrum up to $200 Z_R = 53$ cm and the color-tuned modes greatly increase in intensity.

In these cases the energy of the emitted radiation is of relatively long wavelength. For $m = 1$ we have 5.9 μm for non-tuned and 12.2 μm for color-tuned modes and then for $m = 3$ we have 1.97 μm for non-tuned and 2.5 μm for color-tuned, owing to the low energy electron. Shorter wavelengths can be achieved by using higher energy electrons.

V. HIGH-ENERGY, COLOR-TUNED SYNCHROTRON SOURCE

In order to achieve higher frequencies we will consider a higher energy electron bunch with $\gamma_0 = 1000$. The challenge with higher energy electron bunches is that dephasing between the bunch and the laser becomes an issue. In general, the dephasing length for a Hermite-Gaussian mode,

$$L_d \approx \frac{1}{2} \frac{\lambda_p^3}{\lambda^2} \left[1 + \kappa^2(m + n + 1) \right]^{-1},$$
(31)

is on the order of the slippage length when operating at the plasma resonance, i.e., $L \approx r_0 \approx \lambda_p/\pi$, such that
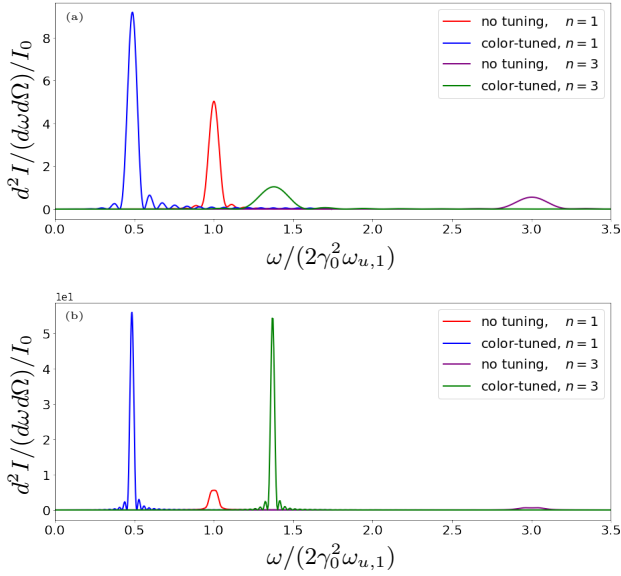
FIG. 5. The spectra corresponding to the trajectories in Fig. 4. Panel (a) corresponds to an integration of the energy up to slippage lengths $L_s = 81Z_R$ for $m = 1$ and $L_s = 27Z_R$ for $m = 3$ while panel (b) to an integration up to $200Z_R$ for both. The red spectrum corresponds to non-tuned $m = 1$ wakefield, blue to color-tuned $m = 1$ wake, purple to non-tuned $m = 3$ wake, and the green to $m = 3$ color-tuned wake. The dashed black line demarcates the slippage length at $81Z_R$ for a non-tuned $m = 1$ mode.

$L_s/L_d \approx (k_p L)(k_p r_0)^2/[2\pi|(m_1 + n_1) - (m_2 + n_2)|] = 4/[\pi|(m_1 + n_1) - (m_2 + n_2)|]$, and so cannot be ignored for even a moderate energy electron bunch, i.e., $\gamma_0 = 1/\sqrt{1 - \beta_\text{bunch}^2} \lesssim 100$. From this we can deduce that higher-order modes will be less impacted by dephasing than lower-order modes, which is desirable since higher-order modes will also generate higher undulator frequencies.

Dephasing for a high-energy bunch can be addressed by using Eqs. (A1) and (A5) to taper the plasma channel with respect to density and curvature. Using this channel profile we model an electron bunch of 1000 particles injected into the wake of a color-tuned, multimode pulse. Likewise, since the spotsize is changing we must also modify the modal contributions so that energy is conserved, i.e., $C_0 \to C_0/\hat{r}$ and $C_m \to C_m/\hat{r}$. In this case we will use $m = 0$ and $m = 7$ modes, where $\lambda_7 = 581$ nm, and a bunch of initial energy $\gamma_0 = 1000$, zero energy spread $\Delta E/E = 0$, and average spot size $\sigma_x = \langle x \rangle = 0.1$ μm and corresponding average momentum $\sigma_{p_x} = \gamma_0 k_{\beta_x}\langle x \rangle$, giving a normalized transverse emittance of $\epsilon_x = \frac{1}{m_e c}\sqrt{\langle x^2\rangle\langle p_x^2\rangle - \langle xp_x\rangle^2} = 0.32$ μm. Similar numerical parameters as before are used except now the modes are initialized to $C_0 = 0.1$ and $C_7 = 0.9C_0/\sqrt{35/8}$, where we allow for explicit betatron oscillations for a more realistic bunch. The bunch is initialized at $k_p\zeta_0 = -21\pi/2$ and $x_0 = a_u(k_7)/(\gamma_0 k_{u,7})$. The undulator strength parameter for this setup is $a_u = 0.34$
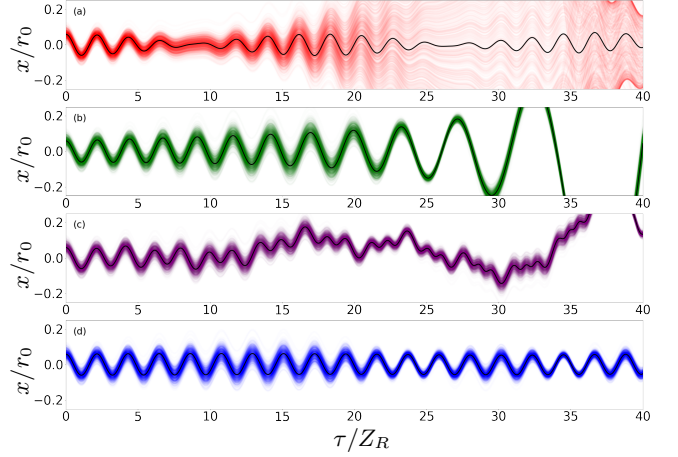

FIG. 6. The trajectories of a bunch of 1000 test electrons in the wake of an $m = 0$ and $m = 7$ laser driver with various channel taperings: (a) no channel tapering, (b) only density tapering, (c) tapering of the channel density and radius so that the bunch is fixed with respect to the phase of both the transverse and longitudinal fields, and (d) tapering of density and radius such that the bunch is fixed with respect to the transverse fields but also so that the undulator frequency ω_u remains constant.

and there will be a small contribution due to betatron motion, $a_\beta = \gamma_0 k_{\beta x} x_{bx} = 0.02$, where x_{bx} is the average oscillation amplitude of the electron trajectory (we are neglecting oscillations in the y plane).

The resulting trajectories can be seen in Fig. 6 for four different conditions, where the average orbits per bunch are plotted in black. For a longitudinally uniform parabolic channel the bunch will pass through different phases of the wake and beat between two different frequencies (red) until expelled from the wake by the defocusing force of the wake. Simple tapering of the density in Fig. 6(a), using Eq. (A1) with constant channel radius $r_s = r_0$, is not sufficient to have a properly radiating bunch, resulting in an increasing undulator wavelength until eventual particle loss (green) in Fig. 6(b). The use of density tapering and matched channel radius variation in order to fix the fields with respect to the electron, Eqs. (A1) and (A4), will initially guide the particle at the proper frequency but eventually the wavelength will begin to decrease until the particle is lost again (purple), Fig. 6(c). The use of density tapering in Fig. 6(d), Eq. (A1), but with proper variation of the channel radius, Eq. (A5), results in guided propagation with constant undulation frequency ω_u. This particle will propagate until it reaches the dephasing limit z_s and is subsequently lost. The spectra for these trajectories can be seen in Fig. 7. Using proper tapering allows for a clean and intense peak at a wavelength of $\lambda_{u,7} = 3.12$ nm (solid blue line) over the course of $N_u = 18$ betatron periods. The total emitted photons per electron per undulator period in this case is $N_p = 0.0024$ and the collimation angle is $\theta_n = 0.24$ mrad.
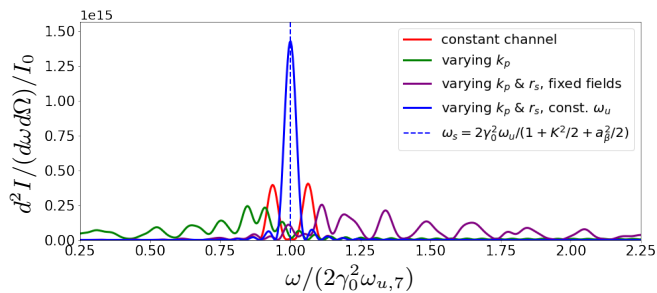
FIG. 7. The spectra corresponding to the trajectories in Fig. 6

VI. CHIRPED SYNCHROTRON PULSES

Typically in a synchrotron one requires a constant undulator frequency to maximize the emitted radiation. However, a tapered plasma channel can also use dephasing to slowly modify the undulator frequency and introduce a controlled chirp to the generated synchrotron radiation. This is accomplished using Eqs. (A6) and (A7) which have been modified so that one may arbitrarily tune the slope of $\hat{k}_p$ and $\hat{r}$ by introducing tuning parameters α_{k_p} and α_r via $\epsilon \to \alpha_{k_p}\epsilon$ and $K_m \to (\alpha_r/\alpha_{k_p})K_m$. For this problem, $m = 0$ and $m = 11$ modes will be used, with $\lambda_{11} = 513$ nm, and again an electron of initial energy $\gamma_0 = 1000$. The bunch will be initialized at $k_p\zeta_0 = -41\pi/2$, $x_0 = a_u(k_{11})/(\gamma_0 k_{u,11})$, and $\sigma_\beta = 0.1\mu m$ and the modes to $C_0 = 0.1$ and $C_{11} = 0.9C_0/\sqrt{693/128}$. The initial undulator strength parameter for this case is $a_u = 0.207$ but varies as the plasma density changes.

The results for this numerical setup can be seen in Fig. 8, where the average orbit per bunch is plotted in black. In Fig. 8(a) is plotted the full numerical solution of Eqs. (A1) and (A5) (blue) and in Fig. 8(b) we have the linear taper for Eqs. (A6) and (A7) (orange) with $\alpha_{k_p} = \alpha_r = 1$. Note that Fig. 8(b) demonstrates that a linear taper is an acceptable approximation to Fig. 8(a). In Fig. 8(c) we have $\alpha_{k_p} = 1$ and $\alpha_r = 5$ for the linear taper (pink), causing the wavelength of the undulator to rapidly decrease. In Fig. 8(d) we have $\alpha_{k_p} = 1.1$ and $\alpha_r = 0$ (turquoise), causing the undulator wavelength to increase. Fig. 9 shows the energy spectra for the four trajectories, and in Fig. 10 shows the time-frequency spectra. There is a peak at $\omega_s = 2\gamma_0^2\omega_{u,11}/(1 + a_u^2/2 + a_\beta^2/2)$. The $\alpha_r = 5$ case yields a negatively chirped spectrum while $\alpha_r = 0$ yields a positive chirp. The slope and width of the chirp can also be tuned by varying the initial values of ψ_0 and κ. The peak wavelength in all three cases is $\lambda_{u,11} = 2.25$ nm.

VII. SUMMARY AND CONCLUSIONS

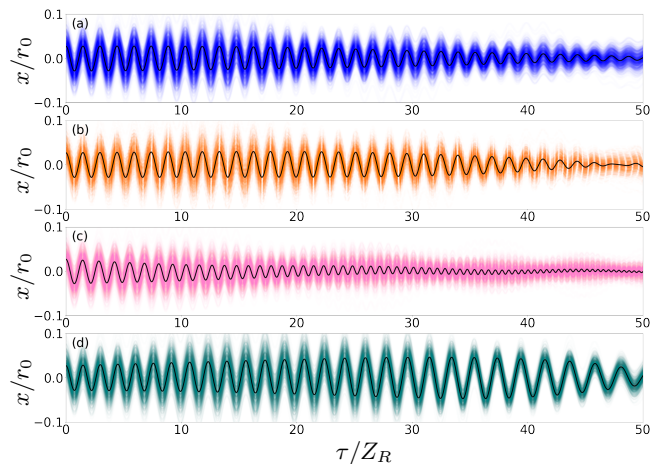In this paper we propose using color tuning to optimize the plasma undulator concept as an alternative to

FIG. 8. The trajectories of a bunch with N=1000 test particles in a channel linearly tapered with respect to density and radius: (a) a nonlinearly tapered channel Eqs. (A1) and (A5), (b) a linear taper with $\alpha_{k_p} = 1$ and $\alpha_r = 1$, (c) $\alpha_{k_p} = 1$ and $\alpha_r = 5$, and (d) $\alpha_{k_p} = 1.1$ and $\alpha_r = 0$.
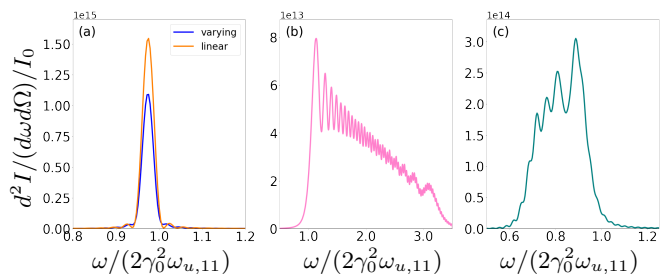

FIG. 9. The energy spectra corresponding to the trajectories in Fig. 8. In (a) we compare the spectra from an optimal, numerically-determined, density taper (blue) versus a linear taper (orange). The energy spectrum in (b) corresponds to a positive chirp in frequency while (c) corresponds to a negative chirp.

traditional, magnetic-undulator based synchrotron systems. Using the fact that two modes of different geometric mode numbers can copropagate at the same group velocity, if their respective wavenumbers are appropriately chosen, we are able to overcome the limitation of mode slippage. This analysis is done in the Hermite-Gaussian basis, but a similar formulation can be made also in cylindrical coordinates. Initially using single particle motion for a low energy electron, so that its group velocity is the same as that of the laser in a plasma, we compared the radiation spectrum from non-tuned and color-tuned orbits for $m = 1$ and $m = 3$ modes. In order to generate soft X-rays, we provided another example for a higher-energy bunch of $\gamma_0 = 1000$ propagating through the wake of an $m = 7$ mode. In order to overcome dephasing, we tapered the plasma density longitudinally and did so such that the undulator frequency would not be modified by the changing plasma wavelength. Lastly, we provided an
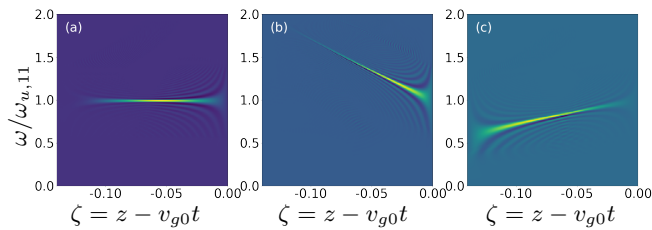
FIG. 10. The time-frequency spectra corresponding the trajectories in Fig. 8: (a) the trajectory from the linear tapering, (b) positive chirp, (c) negative chirp.

example of how linear tapering can be used to generate chirped X-ray pulses. In both high energy cases nanometer scale radiation was produced.

Experimental implementation of a color-tuned undulator depends on several factors. First, it is necessary to have advanced control over the phase and polarization of individual laser modes. Furthermore, there must be an accessible way to create specific higher-order modes at high intensities, although this can be relaxed if additional radiation from betatron oscillations is not a concern. Likewise, one must select modes that correspond to laser frequencies that can be readily generated using modern laser technology. Ti:Sapphire lasers typically have a wide wavelength range from 650 nm - 1150 nm, allowing for a single system to generate the necessary mode content. Once these criteria are met it will be important to take into consideration how different modes will be aligned and combined, possibly by means of fiber optics. Lastly, if one were to use high energy electron bunches, greater control over the plasma channel profile both transversely and longitudinally will be necessary.

Advanced light source technology is one of the most promising applications of LPA research and can be achieved by coupling an LPA to either a traditional magnetic undulator or to a plasma-based undulator as proposed in this manuscript. While magnetic based systems are currently well understood, a plasma-based system will be far more compact and manageable, allowing for advanced X-ray spectroscopy in a university laboratory as well as potential biomedical applications. An additional potential application would be to XUV lithography, as a plasma-based light source would provide a cheap and compact means of precision optical etching.[21] Future work could include further exploring a more rigorous formulation, without assumptions on the transverse scale lengths. This may be important since higher-order modes have much steeper gradients that may be contributing nonlinearly to the evolution of the wakefields and the particle trajectories. Likewise, a more rigorous description of redshifting could be incorporated as well as the three-wave interactions between two modes of different colors and the plasma and how that might affect this approach to a plasma undulator.

VIII. ACKNOWLEDGMENTS

Appendix A: Dephasing in the color-tuned regime

In order to compensate for dephasing we need to use a longitudinally tapered density profile. There are several approaches one can consider, but in all cases we need to identify a solution which preserves the relative phase of the electron with respect to the wakefields,[22] in our case prioritizing the transverse fields over the longitudinal fields. In order to do this we use the following differential equation to govern the taper of the density profile of the plasma:

$$\frac{d\hat{k}_p}{d(\tau/Z_R)} = \epsilon \hat{k}_p^2 \left(\hat{k}_p^2 - \frac{1}{2}\frac{\kappa^2}{\hat{r}^2} \right), \qquad (A1)$$

where $\hat{k}_p = k_p(\tau)/k_{p0}$, $\epsilon = k_{p0}^3 Z_R/(2|\psi_0|k^2)$, and note that k_p is a function of propagation distance τ, $\psi_0 = k_{p0}\zeta_0$, $\hat{r} = r_s(\tau)/r_0 = R(\tau)/R(0)$, $\kappa = 2/(k_{p0}r_0)$, where the laser spot size r_s varies with the channel radius R. Higher-order, color-tuned modes dephase at the same rate as the Gaussian mode of wave number k. When assuming a constant or slowly varying spot size $\hat{r}$, we can approximate the general solution as

$$z_s(\hat{k}_p) = \frac{Z_R}{\epsilon\sqrt{2}} \left\{ \frac{1}{\hat{k}_p} - 1 + \frac{\sqrt{2}}{\kappa} \left[\text{atanh}\left(\frac{\sqrt{2}}{\kappa}\right) - \text{atanh}\left(\frac{\sqrt{2}\hat{k}_p}{\kappa}\right) \right] \right\}, \qquad (A2)$$

and the point at which the density becomes singular,

$$z_s = \frac{Z_R}{\epsilon\kappa^2} \left\{ \frac{\sqrt{2}}{\kappa} \log\left[\left(1 + \frac{\sqrt{2}}{\kappa}\right) \Big/ \left|1 - \frac{\sqrt{2}}{\kappa}\right| \right] \right\}. \quad (A3)$$

Transverse field phase locking can be extended to the longitudinal fields as well by coupling the density profile to a differential equation for the spot size (and corresponding channel radius):

$$\frac{d^2\hat{r}}{d(\tau/Z_R)^2} = \frac{1}{\hat{r}^3}(1 - \hat{k}_p^2\hat{r}^2). \qquad (A4)$$

However, we will be sacrificing longitudinal phasing in our case, as the distortion of the fields would in turn vary the undulator wavelength. In order to preserve the undulator frequency we differentiate Eq. (20) with respect to the propagation variable τ, allowing for r_s and
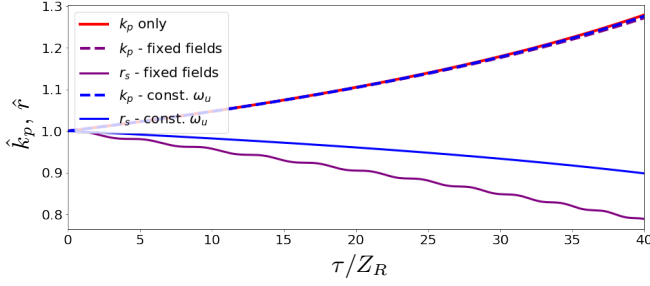
FIG. 11. Plot of the normalized plasma wavenumber $\hat{k}_p$ and channel radius $\hat{r}$ for various longitudinal tapering profile. Density tapering of Eq. (A1) with $\hat{r} = 1$ (red). Tapering of density (dashed purple) and radius (solid purple) such that the bunch is fixed in phase with both the transverse and longitudinal fields, coupled system of Eqs. (A1) and (A4). Tapering of density (dashed blue) and radius (solid blue) such that bunch is fixed with respect to the transverse fields and the undulation frequency ω_u remains constant, Eqs. (A1) and (A5).

k_p to vary, and solve for r_s, yielding:

$$\frac{d\hat{r}}{d(\tau/Z_R)} = \epsilon\kappa_m\hat{k}_p^3\hat{r}^3\left(\hat{k}_p^2 - \frac{1}{2}\frac{\kappa^2}{\hat{r}^2}\right), \qquad \text{(A5)}$$

where $\kappa_m = (k_m - k)/\kappa^2/[k_m - k(m+1)]$. Solving these coupled differential equations (A1) and (A5) will generate a longitudinal density taper and spot-size variation to allow for constant ω_u. This in shown in Fig. 11, where the spotsize decreases as the density increases. Eqs. (A1) and (A5) can be linearized when $z \ll z_s$ with respect to the small parameter ϵ and by making the substitutions $\hat{k}_p = 1 + \epsilon\hat{k}_{p1}$ and $\hat{r} = 1 + \epsilon\hat{r}_1$, yielding:

$$\hat{k}_p(\tau) = 1 + \epsilon(1 + \kappa^2)(\tau/Z_R), \qquad \text{(A6)}$$

$$\hat{r}(\tau) = 1 + \epsilon K_m(1 + \kappa^2)(\tau/Z_R). \qquad \text{(A7)}$$

These equations are valid on the length scales in consideration and allow for ready implementation and tuning of a tapered plasma channel.

Appendix B: Red-shifting of higher-order modes

For an arbitrary higher-order mode the mean laser number can be expressed as a function of the normalized energy and the wave action as $\langle k_m/k\rangle = \mathcal{E}/\mathcal{A}$, where $\mathcal{A}$ is the action.[23] The initial rate of change in energy can be approximated as

$$\left.\frac{\partial\mathcal{E}}{\partial\tau}\right|_{\tau=0} \simeq -\frac{k_p^5}{2k_m^2}\int d\zeta\int dr r\frac{\partial\rho}{\partial\zeta}|a|^2, \qquad \text{(B1)}$$

where $\rho = n/\gamma_0 n_0 = (1+\phi)^{-1}$. Normalizing with respect to the Gaussian energy,

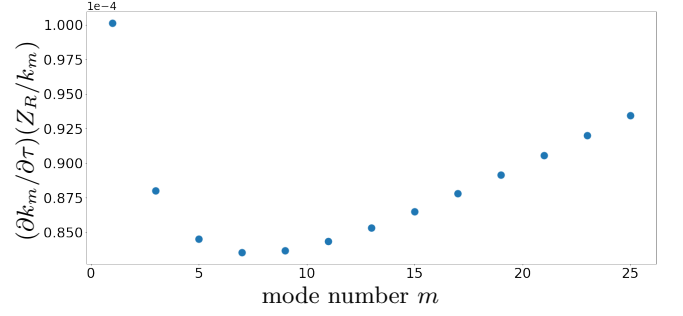$$\mathcal{E}_0 \simeq \sqrt{\frac{\pi}{2}}k_p L a_0^2\frac{(k_p r_0)^2}{4}, \qquad \text{(B2)}$$

FIG. 12. A plot of $\partial_\tau k_m/k_m$ as a function of mode number m over a distance Z_R for $k_p/k = 0.025$ and $r_0 = 25~\mu$m.

the effective change in wave number is,

$$\frac{1}{k_m}\frac{\partial k_m}{\partial\tau} = \mathcal{E}_0^{-1}\frac{k_p^4}{2k_m^2}\int\int\frac{1}{4}\left(a^2 - \frac{1}{k_p^2}\nabla_\perp a^2\right)a^2\mathcal{F}dxdy. \qquad \text{(B3)}$$

Here

$$\mathcal{F} = k_p^2\int_{-\infty}^{\infty}d\zeta\int_{\zeta}^{\infty}d\zeta'\cos[k_p(\zeta - \zeta')]g^2(\zeta)g^2(\zeta')$$
$$\approx \frac{\pi}{4}k_p^2 L^2 e^{-L^2/4}, \quad \text{(B4)}$$

and $g(\zeta) = \exp[-(\zeta - \zeta_0)^2/L^2]$ is the longitudinal profile of the laser mode. The variation of $\partial k_m/\partial\tau$ as a function of mode number is shown in Fig. 12 for $k/k_p = 0.025$. For typical parameters very little energy is depleted over a Rayleigh range and laser red-shifting is not a major concern in a plasma undulator.

[1] D. Attwood and A. Sakdinawat. *X-Rays and Extreme Ultraviolet Radiation: Principles and Applications.* Cambridge University Press, Cambridge, 2016.

[2] P. Emma, R. Akre, J. Arthuer, et al. *Nature Photonics*, 4:641, 2010.

[3] W. Ackermann et al. *Nature Photonics*, 1:2007, 2007.

[4] T. Wolf et al. *Nature Chemistry*, 11:504–509, 2019.

[5] C. Pellegrini, A. Marinelli, and S. Reiche. *Rev. Mod. Phys.*, 88: 015006, 2016.

[6] T. Clarke. *The Science and Technology of Undulators and Wigglers.* Oxford University Press, New York, 2004.

[7] E. Esarey, B.A. Shadwick, P. Catravas, and W.P. Leemans. *Phys. Rev. E*, 65:056505, 2002.

[8] F. Albert et al. *Phys. Plasmas*, 25:056706, 2018.

[9] S. Rykovanov, C.B. Schroeder, E. Esarey, C.G.R. Geddes, and W.P. Leemans. *Phys. Rev. Lett.*, 114:145003, 2015.

[10] S. Rykovanov, J.W. Wang, V. Yu Kharin, B. Lei, C.B. Schroeder, C.G.R. Geddes, E. Esarey, and W.P. Leemans. *Phys. Rev. Acc. & Beams*, 19:090703, 2016.

[11] J.W. Wang, C.B. Schroeder, R. Li, M. Zepf, and S.G. Rykovanov. *Nature Sci. Rep.*, 7:16884, 2017.

[12] S.-C. Chu, Y.-T. Chen, K.-F. Tsai, and K. Otsuka. *Opt. Express*, 20, 2012.

[13] G.A. Turnbull, D.A. Robertson, G.M. Smith, L. Allen, and M.J. Padgett. *Opt. Commun.*, 127, 1996.

[14] Y. Shen, Y. Meng, X. Fu, and M. Gong. *Opt. Lett.*, 43, 2018.

[15] E. Cormier-Michel, E. Esarey, C. G. R. Geddes, C. B. Schroeder, K. Paul, P. J. Mullowney, J. R. Cary, and W. P. Leemans. *Phys. Rev. Acc. and Beams*, 14:031303, 2011.

[16]B.Z. Djordjević, C. Benedetti, C.B. Schroeder, E. Esarey, and W.P. Leemans. *Phys. Plasmas*, 26:013107, 2019.

[17]T. Tajima and J.M. Dawson. *Phys. Rev. Lett.*, 43, 1979.

[18]E. Esarey, P. Sprangle, J. Krall, and A. Ting. *IEEE J. Quantum Electron.*, 33:1879, 1997.

[19]E. Esarey, C.B. Schroeder, and W.P. Leemans. *Rev. Mod. Phys.*, 81:1229, 2009.

[20]E. Esarey, P. Sprangle, M. Pilloff, and J. Krall. *J. Opt. Soc. Am. B*, 12, 1995.

[21]B. Newman. *Opt. Engineering*, 30:1100, 1991.

[22]W. Rittershofer, C.B. Schroeder, E. Esarey, F.J. Grüner, and W.P. Leemans. *Phys. Plasmas*, 17, 2010.

[23]C. Benedetti, F.Rossi, C.B. Schroeder, E.Esarey, and W.P. Leemans. *Phys. Rev. E*, 92:023109, 2015.